Published in : J. Struct. Eng.(2024), 150(9), 04024122
DOI: 10.1061/JSENDH.STENG-12984
Status : Postprint (Author's version)

Buckling Strength of Rolled Angles: Comparison between International Codes

Hamdy Farhoud, S.M.ASCE[1]; Marios-Zois Bezas[2]; Jean-François Demonceau[3]; Jean-Pierre Jaspart[4]; and Ioannis Vayas[5]

[1]*Ph.D. Student, Dept. of Civil and Environmental Engineering, Henry M. Rowan College of Engineering, Rowan Univ., Glassboro, NJ 08028 (corresponding author). ORCID: https://orcid.org/0000-0001-7696-404X*
[2]*Postdoctoral Researcher, Steel and Composite Construction, Urban and Environmental Engineering (UEE) Research Unit, Liège Univ., Liège 4000, Belgium. ORCID: https://orcid.org/0000-0001-5014-3569*
[3]*Professor, Steel and Composite Construction, Urban and Environmental Engineering (UEE) Research Unit, Liège Univ., Liège 4000, Belgium. ORCID: https://orcid.org/0000-0002-0988-8929*
[4]*Professor, Steel and Composite Construction, Urban and Environmental Engineering (UEE) Research Unit, Liège Univ., 4000 Liège, Belgium. ORCID: https://orcid.org/0000-0003-1496-6300*
[5]*Emeritus Professor, School of Civil Engineering, Institute of Steel Structures, National Technical Univ. of Athens, Athens 15772, Greece. ORCID: https://orcid.org/0000-0002-2898-3286*

Abstract: Angle profiles belong to the most common steel profiles used in several types of civil engineering structures, such as in lattice towers. Although, in such towers, they are usually considered as axially loaded (truss) members, an additional bending moment develops due to the eccentricity between the point of load application and the gravity center of the profile. Therefore, this paper focuses on the buckling resistance of single-angle members subjected to combined compression and bending. The investigations have been performed through numerical parametrical studies and have been compared to different normative documents where interaction equations are provided.

Keywords: Equal-leg rolled angles; Stability of members; Buckling; Numerical simulations; Eurocode 3; AISC.

Introduction

Steel lattice towers constitute a substantial part of the telecommunication and electrical infrastructure worldwide. Their construction is expected to accelerate in view of recent developments in 5G technology and clean energy power production. These towers are usually made of hot-rolled or cold-formed equal-leg steel angles profiles that are assembled to form a framework. The connections through bolts and gusset plates allow a modular construction of the tower and, therefore, simplifies its erection at the construction site. However, the cross-sectional geometry and the connection on one leg introduce an eccentricity and, as a result, an additional bending moment to the member.

Nowadays, different normative documents may be used for the design of angle members. Eurocode 3 does not cover the design of angles in a single document but provides rules and recommendations in various parts. The general part, EN1993-1-1 (CEN 2005), and its next version, FprEN1993-1-1 (CEN 2022), provide rules for cross-sectional classification and stability verifications of members. However, the latter does not refer to angle profiles. The buckling resistance of rolled or welded class-4 angles subjected to compression is determined by EN1993-1-5 (CEN 2006a), while EN1993-1-3 (CEN 2006c) covers cold-formed angles. Lattice towers are dealt with in EN1993-3-1 (CEN 2006b), which gives specific rules for the buckling resistance of angle members accounting for the connection eccentricity to one leg and the relevant restraint effect. A new version of the Code, prEN1993-3 (CEN 2021), is currently being edited. It includes in its Annex F general rules for the design of angle profiles, based on the outcomes and results of the recently completed European Research Fund for Steel and Coal–funded project ANGELHY (Vayas et al. 2021). Another European specification, the CENELEC standard EN50341-1 (CEN 2012) dealing with transmission towers, includes design rules for angle members that also account for the effects of end

Published in : J. Struct. Eng.(2024), 150(9), 04024122
DOI: 10.1061/JSENDH.STENG-12984
Status : Postprint (Author's version)

connections, although sometimes differently than EN 1993-3-1. Finally, rules can be found in the American Codes, where contrary to the Eurocodes, are presented in a single document named ANSI/AISC-360-22 (ANSI/AISC 2022); the historic LRFD specification for angles (Fisher 2000) has also been suspended to the general standard.

The behavior of angle sections and members has been studied both analytically and experimentally. Može et al. (2014) investigated, both experimentally and numerically, the influence of the residual stresses distribution of equal-leg angle profiles to their buckling resistance. Vayas et al. (2009) gave the inelastic capacity of angle sections to combined axial forces and biaxial bending, while Kettler and Unterweger (2019) highlighted the importance of the end support conditions in their numerical studies of rolled angles loaded in compression through bolted connections in one leg and in their comparisons with experimental results and with the provisions of the European standards. Bezas et al. (2022, 2021a) proposed a fully validated set of consistent design rules for angles, covering all aspects of design such as classification, cross section, and member resistance under different load combinations. Liang et al. (2019) and Behzadi-Sofiani et al. (2021) investigated, both experimentally and numerically, the influence of the fixed-ended boundary conditions to the buckling resistance of equal-leg angle profiles that are subjected to concentric compression loads; however, both studies referred to stainless steel angles. Finally, extensive experimental investigations including hot-rolled angles ranging from regular to high-strength steel grades have also been carried out by various authors (Ban et al. 2013; Bezas et al. 2021b; Shi et al. 2012; Spiliopoulos et al. 2018).

This paper studies the buckling resistance of single-angle members subjected to combined compression and bending. A large number of numerical parametrical studies on hot-rolled steel angles have been conducted by means of the full nonlinear software ABAQUS, considering geometrical and material nonlinearities. The influence of different modeling parameters on the member response, such as the type of the finite element and the shape and magnitude of the initial imperfections, in correspondence with the relevant buckling modes, were investigated. Subsequently, the numerically obtained results were compared with the provisions of both prEN 1993-3, Annex F, and AISC 360-16 for combined compression and bending. Furthermore, in the latest version of EN 1993-1-3 known by the authors, prEN1993-1-3 (CEN 2020), it is reported in clause 8.2.5 that the interaction formulae given for the buckling resistance of cold-formed members subjected to compression and biaxial bending may also be applied to hot-rolled and welded sections. Based on this suggestion, the numerical results were also compared to the predictions of that Code. However, it should be clarified that there is no general validation of the prEN 1993-1-3 interaction formulae on cold-formed sections but only its application to the hot-rolled ones, and specifically to angles. The aim of these comparisons is to check the adequacy of the provisions of the considered standards about the design of angle members subjected to compression and biaxial bending, because most of them are quite new. The work presented here is a part of the work carried out in the framework of the master thesis of the first author (Farhoud 2022).

Both European and American normative documents are used in this paper and their symbols are defined in the "Notation." To make the distinction of the symbols amongst them easier, the term "AC" has been added to the symbols referring to the American standard. Despite this distinction, the notations and wordings of the original norms have been kept in the paper even though, in some cases, they appear contradictory.

Cross-Sectional Classification

As we deal with different normative standards, three classification systems have been considered as follows:

1. The one given in prEN 1993-1-1 that applies in combination with prEN 1993-1-3. Although both local and distortional buckling modes should be taken into account according to prEN 1993-1-3, the distortional one is not relevant here because only hot-rolled profiles have been considered.
2. The one provided in prEN 1993-3-Annex F. Despite that the ratio h-2t/t is suggested to be used by prEN 1993-3, the ratio c=t has been used here, which gives similar results (Bezas et al. 2021a).
3. The one proposed by ANSI/AISC-360-22 (ANSI/AISC 2022).

In all documents, the criteria are based on the same geometric and material properties such as ε, c, and t. In contrast with the Eurocodes, the ANSI/AISC 360-22 classifies the sections into three classes: compact, noncompact, and slender-element sections; the relevant criteria are reported in Eqs. (1) and (2). Fig. 1 shows the notations for the geometrical properties, as well as the geometrical and the principal axes.

Published in : J. Struct. Eng.(2024), 150(9), 04024122
DOI: 10.1061/JSENDH.STENG-12984
Status : Postprint (Author's version)

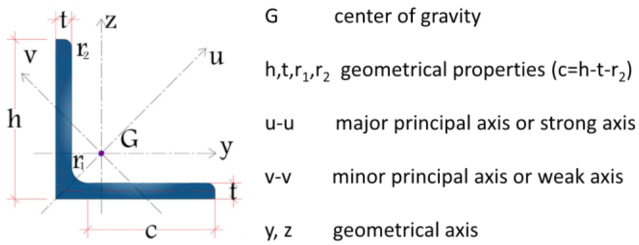

Fig. 1. Notations for geometrical properties and principal axes.

For axial compression:

The section is noncompact if $\frac{h}{t} \leq 0.45\sqrt{\frac{E}{F_y}}$

The section is slender if $\frac{h}{t} > 0.45\sqrt{\frac{E}{F_y}}$ (1)

For flexure about strong and/or weak axis:

The section is compact if $\frac{h}{t} \leq 0.54\sqrt{\frac{E}{F_y}}$

The section is noncompact if $0.54\sqrt{\frac{E}{F_y}} < \frac{h}{t} \leq 0.91\sqrt{\frac{E}{F_y}}$

The section is slender if $\frac{h}{t} > 0.91\sqrt{\frac{E}{F_y}}$ (2)

Design Rules for Angles Members

Provision of prEN 1993-1-3

In prEN 1993-1-3, specific criteria to evaluate the design resistance against combined axial force and biaxial bending are given. Even though those rules have been developed for cold-formed sections, it is clearly stated that they may also be used for hot-rolled ones. Buckling to compression and bending is checked by means of the following two interaction equations. Values for the exponents and of the interpolation factors are provided in prEN1993-1-3. Here, their conservative values given in prEN1993-1-3 have been adopted (i.e., $\omega x_{,}u = \omega x_{,}v = \omega x,LT = 1.0$ and $au = av = \beta u = \beta v = \delta u = \delta v = 0.85$)

Published in : J. Struct. Eng.(2024), 150(9), 04024122
DOI: 10.1061/JSENDH.STENG-12984
Status : Postprint (Author's version)

$$\left(\omega_{x.u}\frac{N_{Ed}}{\chi_u N_{c.Rd}}\right)^{\alpha_u} + \left(\omega_{x.LT}\frac{M_{u.Ed}+\Delta M_{u.Ed}}{\chi_{LT} M_{cu.Rd}}\right)^{\beta_u} + \left(\frac{M_{v.Ed}+\Delta M_{v.Ed}}{M_{cv.Rd}}\right)^{\delta_u} \leq 1.0 \quad (3)$$

$$\left(\omega_{x.v}\frac{N_{Ed}}{\chi_v N_{c.Rd}}\right)^{\alpha_v} + \left(\omega_{x.LT}\frac{M_{u.Ed}+\Delta M_{u.Ed}}{\chi_{LT} M_{cu.Rd}}\right)^{\beta_v} + \left(\frac{M_{v.Ed}+\Delta M_{v.Ed}}{M_{cv.Rd}}\right)^{\delta_v} \leq 1.0 \quad (4)$$

The design resistances of the cross sections $N_{c;Rd}$, $M_{cu;Rd}$, and $M_{cv;Rd}$ are presented in the following section.

Cross-Sectional Resistance to Compression

The design cross-sectional resistance to compression may be determined as follows:

$$N_{c.Rd} = \begin{cases} \dfrac{A(f_{yb}+4(f_{ya}-f_{yb})(1-(\bar{\lambda}_e/\bar{\lambda}_{e0})_{max}))}{\gamma_{M0}} \leq \dfrac{Af_{ya}}{\gamma_{M0}}, & for\ A_{eff}=A \\ \dfrac{A_{eff}f_{yb}}{\gamma_{M0}}, & for\ A_{eff}<A \end{cases} \quad (5)$$

In Eq. (5), the average yield stress f_{ya} is used to account for the increasing of the yield stress due to the cold forming procedure. However, because this paper deals only with hot-rolled angle profiles, just the basic yield stress f_{yb} is considered (i.e., $f_{ya} = f_{yb} = f_y$). Then, Eq. (5) rewrites as follows, which is identical with the one provided in prEN 1993-1-1:

$$N_{c.Rd} = \begin{cases} \dfrac{Af_y}{\gamma_{M0}}, & for\ A_{eff}=A \\ \dfrac{A_{eff}f_y}{\gamma_{M0}}, & for\ A_{eff}<A \end{cases} \quad (6)$$

Because hot-rolled angle profiles are not susceptible to distortional buckling, only local buckling should be considered for the evaluation of the effective section area, that may be calculated as follows:

$$A_{eff} = A - 2ct(1-\rho) \quad (7)$$

In order to account for the risk of member buckling, prEN 19931-3 clause 7.6.2 (5) proposes a more accurate but more complex procedure of the evaluation of the plate slenderness. Based on that, the reduction factor ρ should be obtained from EN1993-1-5, where the plate slenderness $\bar{\lambda}_p$ is replaced by $\bar{\lambda}_{p.red} = \bar{\lambda}_p\sqrt{\chi_{\min}}$ where $\sigma_{com,Ed} < f_{yb}=\gamma_{M0}$ is the design compressive stress. However, because χ_{min} is a function of A_{eff} $(\bar{\lambda} = \sqrt{A_{\mathrm{eff}} \cdot f_y/N_{cr}})$, an iteration process is required. This starts with $\chi_{min;0}$ 1.0, calculate the effective area according to the aforementioned equations, and finally the $\chi_{min;1}$, which is used for the next repetition. The iteration stops when the buckling reduction factors $\chi_{min;n-1}$ and $\chi_{min;n}$ converge.

Cross-Sectional Resistance to Strong Axis Bending

The design resistance for angle cross sections subjected to strong axis bending, where f_{ya} ¼ f_{yb} ¼ f_y, may be determined from

Published in : J. Struct. Eng.(2024), 150(9), 04024122
DOI: 10.1061/JSENDH.STENG-12984
Status : Postprint (Author's version)

$$M_{cu,Rd} = \begin{cases} \dfrac{f_y(W_{el,u} - 3(W_{pl,u} - W_{u,el})(1 - (\bar{\lambda}_e/\bar{\lambda}_{e0})_{\max}))}{\gamma_{M0}} \leq W_{pl,u}\dfrac{f_y}{\gamma_{M0}}, & for\ W_{eff,u} = W_{el,u} \\ W_{eff,u}\dfrac{f_y}{\gamma_{M0}}, & for\ W_{eff,u} < W_{el,u} \end{cases} \quad (8)$$

The term $(\bar{\lambda}_e/\bar{\lambda}_{e0})_{\max}$ is the largest value of the slenderness ratio $\bar{\lambda}_e/\bar{\lambda}_{e0}$ over all plane elements comprising the cross section (EN1993-1-5). Because only angle sections have been considered in this study, $\bar{\lambda}_e = \bar{\lambda}_p$ and $\bar{\lambda}_{e0}$ = 0.748. Formulae for the calculation of the elastic and plastic properties for angle sections can be found in Bezas (2022). For strong axis bending, the effective cross section may become nonsymmetric due to the different stresses developed in the legs. This behavior slightly changes the position of the section centroid, the directions of the principal axes, and all cross-sectional properties. Fig. 2 illustrates the stress distribution when the section is subjected to strong axis bending; the ratio between the minimum and maximum stresses acting along the leg in compression (that presented in Table 4.2 of EN1993-1-5) may be given by $\psi = (t + r_1)/h$. The reduction factor ρ_u may be calculated according to EN 1993-1-5 for outstand plated elements like the previous section by using the reduced plate slenderness $\bar{\lambda}_{LT,red} = \bar{\lambda}_{LT}\sqrt{\chi_{LT}}$ instead of $\bar{\lambda}_{LT}$. Again, an iteration process is required.

Cross-Sectional Resistance to Weak Axis Bending

The cross-sectional resistance of angles subjected to weak axis bending depend on whether the tip is in tension or compression, and is expressed by the following equation by assuming again that $f_{ya} = f_{yb} = f_y$:

$$M_{cv,Rd} = \begin{cases} \dfrac{f_y(W_{el,v} + 3(W_{pl,vl} - W_{el,v})(1 - (\bar{\lambda}_e/\bar{\lambda}_{e0})_{\max}))}{\gamma_{M0}} \leq W_{pl,v}\dfrac{f_y}{\gamma_{M0}}, & for\ W_{eff,v} = W_{el,v} \\ W_{eff,v}\dfrac{f_y}{\gamma_{M0}}, & for\ W_{eff,v} < W_{el,v} \end{cases} \quad (9)$$

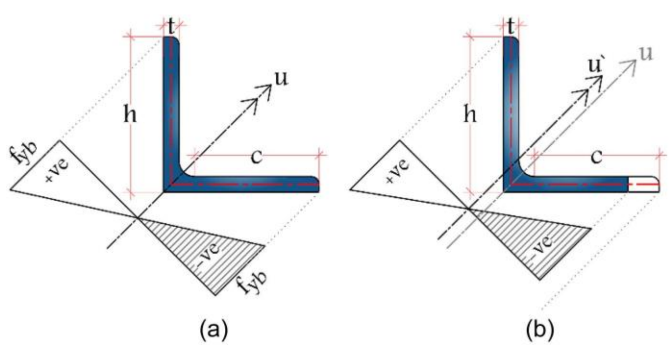

Fig. 2. Stress distribution for strong axis bending: (a) gross section; and (b) effective cross section.

Published in : J. Struct. Eng.(2024), 150(9), 04024122
DOI: 10.1061/JSENDH.STENG-12984
Status : Postprint (Author's version)

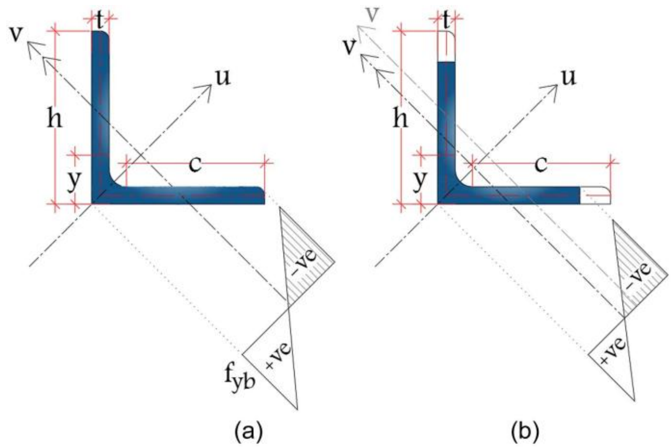

Fig. 3. Stress distribution for weak axis bending (TIC): (a) gross section; and (b) effective cross section.

For weak axis bending when the tip is in compression (TIC), the cross section is still symmetric before and after reduction because the geometric center shifted along the u–u axis. Fig. 3 schematizes the stress distribution when the section is subjected to weak axis bending, and the ratio of end stresses (that presented in table 4.2 of EN1993-1-5) may be given by $\psi = -(y - t - r_1/h - y)$

The reduction factor ρ_v may be calculated according to EN 1993-1-5 for outstand plated elements by using the plate slenderness $\bar{\lambda}_P$, also the plate buckling factor k_σ for outstand compression elements is given in table 4.2 of EN1993-1-5.
The design resistance of angle cross sections when subjected to weak axis bending where the tip is in tension is, in most practical cases, equal to its plastic one.

Buckling Reduction Factors

Reduction Factors for Flexural Buckling χ_v and χ_u. prEN19931-3 states that the reduction factors for flexural buckling (χ_u, χ_v) of cold-formed sections may be calculated according to prEN 19931-1 by using buckling curve c. But because this paper deals with hot-rolled angle profiles, the appropriate buckling curves should be obtained in accordance with prEN 1993-1-1. Subsequently, buckling curve b is used for steel grades less than S460, while buckling curve a for the higher ones.
Reduction Factor for Torsional–Flexural Buckling χ_{TF}. In prEN 1993-1-3, it is indicated that the relevant buckling curve for torsional–flexural buckling may be taken as for flexural buckling (b for steel grades less than S460 and a for the higher ones).
Reduction Factor for Lateral–Torsional Buckling χ_{LT}. According to prEN 1993-1-1 clause 8.3.2.3 and for the reasons already explained, buckling curve d has been used for the evaluation of the reduction factor for lateral–torsional buckling χ_{LT}.

Provision of prEN 1993-3

As aforementioned, in prEN 1993-3, a specific annex (Annex F) is presently providing additional rules and recommendations for the design of angle profiles. Their validation, as well as their background, can be found in Bezas et al. (2022, 2021a). However, a correction has been brought to the interaction equations of prEN1993-3

in order to account for the additional bending moment that develops in class-4 profiles (i.e., the term ΔM_v has been added) due to the movement of the neutral axis

$$\left(\frac{N_{Ed}}{\frac{\chi_u N_{Rk}}{\gamma_{M1}}} + k_{uu}\frac{M_{u,Ed}}{\frac{\chi_{LT} M_{u,Rk}}{\gamma_{M1}}}\right)^{\xi} + k_{uv}\frac{M_{v,Ed} + \Delta M_{v,Ed}}{\frac{M_{v,Rk}}{\gamma_{M1}}} \leq 1.0 \qquad (10)$$

$$\left(\frac{N_{Ed}}{\frac{\chi_v N_{Rk}}{\gamma_{M1}}} + k_{vu}\frac{M_{u,Ed}}{\frac{\chi_{LT} M_{u,Rk}}{\gamma_{M1}}}\right)^{\xi} + k_{vv}\frac{M_{v,Ed} - \Delta M_{v,Ed}}{\frac{M_{v,Rk}}{\gamma_{M1}}} \leq 1.0 \qquad (11)$$

Published in : J. Struct. Eng.(2024), 150(9), 04024122
DOI: 10.1061/JSENDH.STENG-12984
Status : Postprint (Author's version)

Provision of ANSI/AISC 360-22

According to ANSI/AISC-360-22, the interaction equations for combined axial compression and flexure may be given by

$$\frac{P_u}{2\cdot\Phi P_n}-\left(\frac{M_{uw}}{\Phi_b M_{nw}}-\frac{M_{uz}}{\Phi_b M_{nz}}\right)\leq 1 \quad \text{When } \frac{P_u}{\Phi P_n}<0.2 \qquad (12)$$

$$\frac{P_u}{\Phi P_n}+\frac{8}{9}\cdot\left(\frac{M_{uw}}{\Phi_b M_{nw}}+\frac{M_{uz}}{\Phi_b M_{nz}}\right)\leq 1 \quad \text{When } \frac{P_u}{\Phi P_n}\geq 0.2 \qquad (13)$$

In the framework of this paper, the resistance factors (Φ, Φ_b) for both compression and flexure have been taken equal to 1.0, because the code provisions are compared with numerical and experimental results. In contrast to prEN 1993-1-3 and prEN 1993-3, the American interaction equations do not account for the additional bending moment ΔM due to the shift of the centroid of the "noncompact" sections.

Nominal Compressive Strength P_n

The design nominal value of the cross-sectional resistance of a member in compression may be given by

$$P_n=\begin{cases} AF_n, & A_{eff}-A \\ A_{eff}F_n, & A_{eff}<A \end{cases} \qquad (14)$$

The critical stress F_n should be determined according to ANSI/ AISC-360-22 as a function of the slenderness parameter $\lambda_c = \sqrt{F_y/F_c}$ of the compression member, where $F_c = \pi^2E/(KL/r)^2$ is the elastic stress for the relevant buckling mode based on the gross cross-sectional properties

$$F_n=\begin{cases} Q(0.658^{Q\lambda_c^2})F_y, & \lambda_c\sqrt{Q}\leq 1.5 \\ \left(\dfrac{0.877}{\lambda_c^2}\right)F_y, & \lambda_c\sqrt{Q}>1.5 \end{cases} \qquad (15)$$

According to ANSI/AISC 360-22, the reduction factor Q (due to local buckling) for single-angle compression members with slender sections is given by

$$Q=\begin{cases} 1, & \dfrac{h}{t}\leq 0.45\sqrt{\dfrac{E}{F_y}} \\ 1.34-0.761\cdot\dfrac{h}{t}\sqrt{\dfrac{F_y}{E}}, & 0.45\sqrt{\dfrac{E}{F_y}}<\dfrac{h}{t}<0.91\sqrt{\dfrac{E}{F_y}} \\ \dfrac{0.534E}{F_y(\frac{h}{t})^2}, & \dfrac{h}{t}\geq 0.91\sqrt{\dfrac{E}{F_y}} \end{cases} \qquad (16)$$

Fig. 4 illustrates comparisons of the reduction factors ρ and Q for EN 1993-1-5 and ANSI/AISC 360-22, respectively, versus both the plate slenderness $\bar{\lambda}_p$ and the ratio h=t. The Euler's member buckling curve $(\rho_e = \sigma_{cr}/F_y = 1/\bar{\lambda}_p^2)$, the von Kármán $(\rho_{von} = \sqrt{\sigma_{cr}/F_y} = 1/\bar{\lambda}_p)$, as well as the Winter's curve $(\rho_{winter} = 1/\bar{\lambda}_p(1-0.22/\bar{\lambda}_p)$ are reported too. Fot the calculations, a steel grade S235 and a widthρwinter ¼ 1=λpð1 0.22=λpÞ) are reported too. For the calculac approximately equal to 0.9 -· h have been assumed. It can be seen that for the slenderer members where $\bar{\lambda}_p$> 1.30, the reduction factor calculated according to the American standard is quite close to the Euler's elastic factor and more conservative than the one evaluated by the EN

Published in : J. Struct. Eng.(2024), 150(9), 04024122
DOI: 10.1061/JSENDH.STENG-12984
Status : Postprint (Author's version)

1993-1-5, which tends to the Winter and von Kármán curves. On the contrary, for small-to-intermediate slenderness values, both standards provide similar values that tend to Winter's semiempirical curve.

Fig. 5 shows a comparison of different buckling reduction factors calculated by the provision of EN 1993-1-1 and AISC 360-22 for different values of plate reduction factor ρ (0.7 and 1.0) versus the slenderness parameter (λ, λ_c). It can be observed that the American standard does not provide an interaction between local and global buckling for large member slenderness values due to the low limit stress and follows the elastic behavior for any reduction factor for slenderness higher than 1.6.

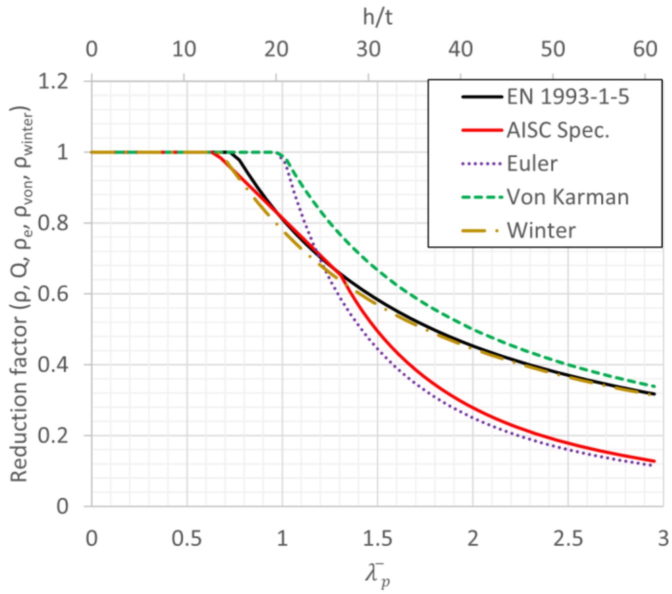

Fig. 4. Comparison of reduction factor (ρ, Q, ρ_e, ρ_{von}, ρ_{winter}) accounting for local buckling as a function of the plate slenderness $\bar{\lambda}_p$ or the h=t ratio.

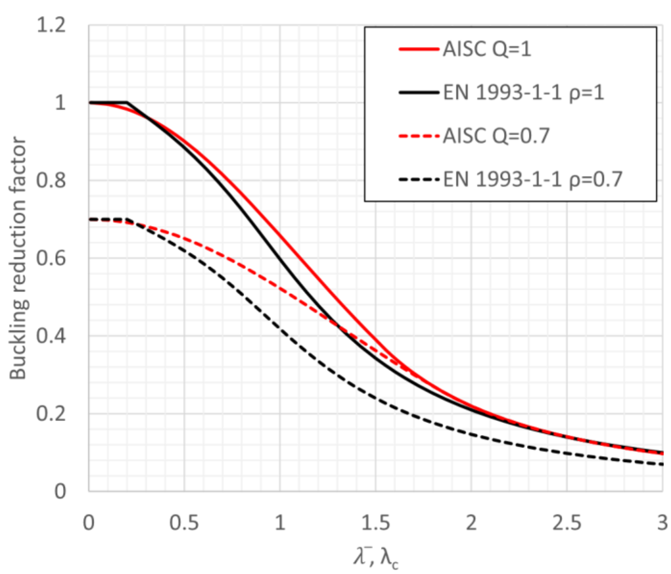

Fig. 5. Comparison of buckling reduction factors as a function of the slenderness parameter (λ, λ_c) for flexural buckling.

Published in : J. Struct. Eng.(2024), 150(9), 04024122
DOI: 10.1061/JSENDH.STENG-12984
Status : Postprint (Author's version)

Nominal Values of Strong Axis Bending M_{nw}

The nominal resistance of major axis bending for angle cross sections is the minimum of the nominal value for local buckling $M_{nw;LB}$ and of the nominal value for lateral–torsional buckling $M_{nw,LTB}$ (i.e., $M_{nw} = \min\{M_{nw;LB};M_{nw;LTB}\}$), where

$$M_{nw,LB} = \begin{cases} 1.5 S_c F_y, & \frac{b}{t} \leq 0.54\sqrt{\frac{E}{F_y}} \\ S_c f_y \left(2.43 - 1.72\left(\frac{b}{t}\right)\sqrt{\frac{F_y}{E}}\right), & 0.54\sqrt{\frac{E}{f_y}} < \frac{b}{t} < 0.91\sqrt{\frac{E}{F_y}} \\ \frac{0.71E}{(\frac{b}{t})^2} S_c, & \frac{b}{t} \geq 0.91\sqrt{\frac{E}{F}} \end{cases} \tag{17}$$

$$M_{nw,LTB} = \begin{cases} \left(1.92 - 1.17\sqrt{\frac{M_y}{M_{cr}}}\right)M_y < 1.5M_y, & M_{cr} > M_y \\ \left(0.92 - 0.17\frac{M_{cr}}{M_y}\right)M_{cr}, & M_{cr} \leq M_y \end{cases} \tag{18}$$

where the critical moment is based on the gross cross-sectional properties and may be calculated by $M_{cr} = C_b\,0.46Eh^2t^2=L$. The bending coefficient C_b is assumed to be equal to 1.0 for this study, because the applied moment is uniformly distributed along the column length in all the considered cases.

A comparison of the ratio of $M_{u;Rk}=M_{u;el}$ calculated by prEN 1993-3, the ratio $M_{nw;LB}=M_y$ calculated by AISC 360-22, Euler's elastic theory $\sigma_{cr}=F_y$, and the von Kármán curve $\sigma_{cr}=F_y$ versus the plate slenderness $\bar{\lambda}_p$ and the ratio h=t is shown in Fig.p 6. For the calculations, steel grade S235 has been adopted while the plate buckling factor k_σ is approximately equal to 1.57 as per Bezas et al. (2021a). It can be observed that the AISC 360-22 provisions seem to be more conservative than the prEN 1993-3 ones after the plastic region (for $\bar{\lambda}_p$ > 0.4), but both tend to the Euler theory.

Published in : J. Struct. Eng.(2024), 150(9), 04024122
DOI: 10.1061/JSENDH.STENG-12984
Status : Postprint (Author's version)

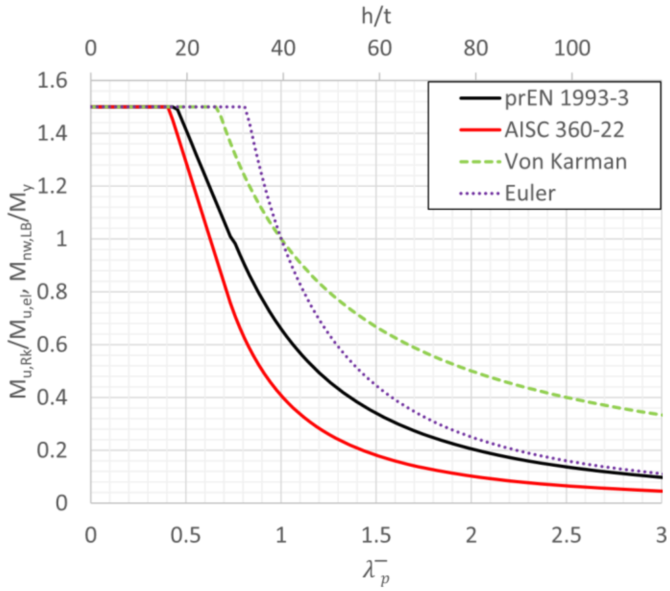

Fig. 6. Comparison of ($M_{u;Rk}$=$M_{u;el}$ and $M_{nw;LB}$=M_y) with ($\bar{\lambda}_p$ and h=t) for strong axis bending.

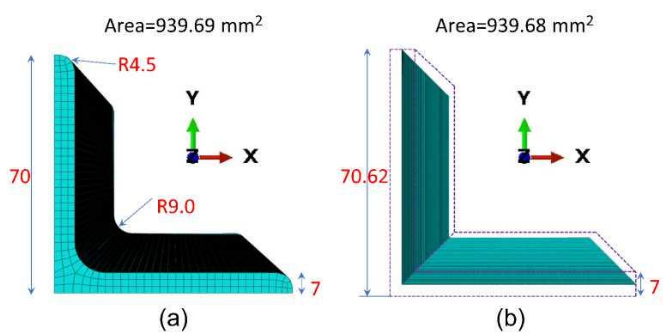

Fig. 7. Numerical model of L70 × 70 × 7: (a) solid FE; and (b) shell FE.

Nominal Values of Weak Axis Bending M_{nz}

The cross-sectional resistance of angles subjected to weak axis bending depends on whether the tip is in tension or in compression. For the former case, the section resistance is the plastic one, while for the latter, the resistance is limited by plate buckling

$$M_{nz} = \begin{cases} \text{Eq. (17)}, & \text{for tip in compression} \\ \mathbf{1.5}\,S_c F_y, & \text{for tip in tension} \end{cases} \tag{19}$$

Numerical Investigations

In order to investigate the sensitivity of various modeling parameters, numerical studies have been performed by means of the full nonlinear software ABAQUS. The numerical results were then compared with experimental tests from the literature performed by Spiliopoulos et al. (2018). Based on these comparisons, a final model was selected and is used hereafter to

Published in : J. Struct. Eng.(2024), 150(9), 04024122
DOI: 10.1061/JSENDH.STENG-12984
Status : Postprint (Author's version)

carry out a large parametrical study, the results of which were then compared with the Code provisions in the "Results and Comparisons" section.

Description of the Numerical Model

Different modeling parameters are investigated in the following, and more particularly the type of the finite element (FE), as well as the shape and amplitude of the initial imperfections. A single angle member L70 × 70 × 7 made of S235 steel was considered as the study case because experimental tests were available to validate the numerical results. In terms of the element type and the cross-sectional geometry, two models have been created for the studied angle: a full one, where the actual shape of the angle section has been simulated by means of solid finite elements, and a simplified one by using shell finite elements, where the fillet radius of the toes and root are not accounted for. For the solid FE model that is schematized in Fig. 7(a), three solid 8-node elements (type C3D8R) per leg thickness have been used, while for the simplified one that is shown in Fig. 7(b), a shell 4-node elements (type S4R) was selected. The simplified model has been chosen to keep the same cross-sectional area and thickness value as the nominal ones; thus, the section height is slightly increasing by 0.89%, which results to an area of A_{shell} =2·(70.62-0.5·7)·7=939,68 mm^2. Although the leg slenderness ratio (c=t) increases by 17.9%, this is not affecting the final result because the studied profile fails through flexural buckling, as explained in this section.

For both models, specific constrains have been implemented at the extremities of the specimens in order to simulate the end plates used by Spiliopoulos et al. (2018) in their tests. These constraints allow for a uniform distribution of the external (concentric or eccentric) applied load and also avoid any local failure at the point of application. At the column top, the displacement in the plane of the cross section (U_X,U_Y) and the rotation about the longitudinal axis of the angle beam (R_Z) were coupled, while at the column base, in addition to the previous ones, the Uz displacement were blocked too. Warping has also been prevented at the end sections due to the applied constraints. Although a considerable strength increase is observed when the secondary warping is prevented at the extremities of equal-leg cold-formed angle members (Shifferaw and Schafer 2014), a similar effect has not been reported for hot-rolled angle sections.

In order to investigate the influence of the shape and amplitude of the initial imperfections to the member's response, different types of geometrical imperfections have been considered in the analyses (see section "Final Numerical Model"):

- A global bow imperfection with a magnitude equal to L½mm=1,000 and a shape similar to the first member instability mode [i.e., flexural or torsional–flexural as it is shown in Figs. 8(b and c), correspondingly]. This value combines approximatively the recommendation of the European norm BSEN1090-2 (BS 2008), which prescribes that the deviation from straightness should be L½mm=750, with the provisions of FprEN1993-1-1 (CEN 2022), which state that 80% of the geometric fabrication tolerances given in BS-EN1090-2 (BS 2008) should be applied.
- A local leg imperfection of h½mm=50 as shown in Fig. 8(a), with a deformable shape affine to the first local buckling mode of the column, obtained through an elastic instability analysis. This value is in line with the recommendation of EN 1993-1-5 Annex C.
- A global bow imperfection of a magnitude equal to L½mm= 5,000 as shown in Fig. 8(b) for flexural or Fig. 8(c) for torsional–flexural buckling. This value corresponds to the actual measured imperfections reported by Spiliopoulos et al. (2018), and will be used only for the validation of the software through experimental results (see Section 4.2).
  An equivalent global imperfection L½mm=700 [Figs. 8(b and c)], which takes into consideration both geometric and residual stresses imperfections as proposed and justified for solid elements in Može et al. (2014).
- A local leg imperfection equal to h½mm=100 as illustrated in Fig. 8(a), which is based on the tolerances defined in EN100562 (CEN 1994), and with imperfection shape in accordance with the first relevant local instability mode.

For all the studied cases, the amplitudes are measured at the most distant node of the deformed shape from the undeformed one. Furthermore, a three-point distribution of residual stresses resulting from the hot-rolling procedure has been contemplated. The selected pattern is chosen from a previous relative study (Može et al. 2014) and is in line with the recommendations of (ECCS 1976).

Published in : J. Struct. Eng.(2024), 150(9), 04024122
DOI: 10.1061/JSENDH.STENG-12984
Status : Postprint (Author's version)

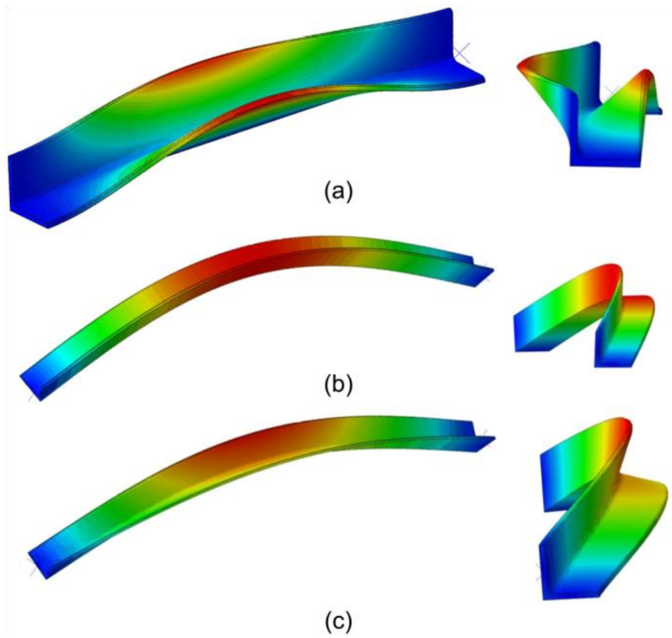

Fig. 8. Typical shape of the geometric imperfection modes of a member with: (a) local buckling; (b) flexural buckling; and (c) torsional– flexural buckling.

Table 1. Details of the tested samples

Length, L (mm)	Eccentricity (mm) e_u	e_v	e_z	Load condition
650	0	0	—	N
650	0	22	—	N + Mu
650	22	0	—	N + Mv
650	—	—	35	N + Mu + M_v
1,170	0	0	—	N
1,170	0	22	—	N + Mu
1,170	5	0	—	N + Mv
1,170	15	0	—	N + Mv
1,170	22	0	—	N + Mv
1,170	—	—	35	N + Mu + Mv
1,750	0	0	—	N
1,750	0	30	—	N + Mu
1,750	30	0	—	N + Mv
1,750	5	0	—	N + Mv
1,750	—	—	35	N + Mu + Mv
2,300	0	0	—	N
2,300	0	30	—	N + Mu
2,300	30	0	—	N + Mv
2,300	5	0	—	N + Mv
2,300	—	—	35	N + M_u + M_v

Source: Data from Spiliopoulos et al. (2018).

Published in : J. Struct. Eng.(2024), 150(9), 04024122
DOI: 10.1061/JSENDH.STENG-12984
Status : Postprint (Author's version)

Comparison of the Numerical Results with Experimental Tests

To validate the accuracy of both models (solid versus shell) and to select the most appropriate shape and magnitude of the initial imperfections to be used afterward, full nonlinear analyses have been conducted and the numerically obtained results were compared with the experimental tests performed by Spiliopoulos et al. (2018). The details of the tested specimens made of L70 × 70 × 7 are summarized in Table 1; the different loading cases due to the eccentric loads are also reported. The experimental stress–strain curve as it has been extracted through coupon tests for the experimental campaign of Spiliopoulos et al. (2018) has been used for the validation of the model, where f_y ¼ 312.93 MPa, f_u ¼ 410.48 MPa, E ¼ 210 GPa, and v ¼ 0.3.

Tables 2–5 presents the experimental (Spiliopoulos et al. 2018) and numerical failure loads for all the specimens and load cases given in Table 1 where different types of elements (solid versus shell), as well as imperfection shapes (i.e., local, flexural, and torsional–flexural) and amplitudes were used. The selected shape of both global and local imperfections is affine to the first considered instability buckling mode (i.e., the first local, the first flexural, and the first flexural–torsional mode) resulting from a linear buckling analysis for the relevant types of loading (concentric or eccentric). Although different shapes were considered in these studies, it should be said that in all cases, the flexural buckling mode was the critical one.
For the numerical investigations, seven cases have been considered in terms of initial imperfections and residual stresses and subsequently reported. Cases 1 to 4 aim to provide information about the influence of the residual stresses on the member response when global or local imperfections are present. Through cases 3 and 5, the influence of the amplitude of a local imperfection is checked while in case 6, the accuracy of an equivalent imperfection is verified. Case 7 seeks to validate the software by using the actual geometrical and material imperfections of the considered experimental tests. The cases are described as follows:

1. (L=1,000): Global imperfection with a magnitude of L=1,000 without residual stresses.
2. (L=1,000 þ RS): Global imperfection with a magnitude of L=1,000 and residual stresses (RS) with the pattern shown in Fig. 8.
3. (h=50): Local imperfection with a magnitude of h=50 without residual stresses.
4. (h=50 þ RS): Local imperfection with a magnitude of h=50 and residual stresses with the pattern shown in Fig. 8.
5. (h=100): Local imperfection with a magnitude of h=100 without residual stresses.
6. (L=700): Global equivalent imperfection with a magnitude of L=700 accounting for residual stresses.
7. (L=5,000 þ RS): Global imperfection with a magnitude of L=5,000 and residual stresses with the pattern shown in Fig. 8; this case is used mainly for the validation of the software because it consists the actual measured initial imperfections reported in Spiliopoulos et al. (2018) (out-of-straightness of the legs were not mentioned).

A tolerance on the position of the applied load from 0 up to 2.0 mm has been adopted for the numerical simulations in order to calibrate the results (only for case L=5,000 þ RS). This tolerance could be justified by the difference between the actual and the nominal position of the load due to the actual geometry of the cross-section, and due to the positioning of the specimen in the testing rig that may also induce a small and unexpected eccentricity, as has been demonstrated by Bezas et al. (2021b) and De Menezes et al. (2019).
For a very few cases, numerical simulations have been performed even in the absence of experimental evidence. This has been done in order to extend the numerical results and to have a clearer view of the investigated modeling parameters.
Fig. 9 shows the axial deformations (shortening) of the specimens with a buckling length of 650 and 1,750 mm versus the load for both experimental tests and numerical simulations (case 7, i.e., L=5,000 þ RS). One can see from the graph that there is a very good agreement between numerical simulations and experimental tests in terms of axial stiffness and load carrying capacity. Similar behavior has been observed for all the specimens.
From these preliminary numerical studies where different modeling aspects have been investigated, the following conclusions may be drawn:

- The numerically obtained resistances for an imperfection value L=5,000 þ RS are on the safe side compared with the experimental ones, with a mean value of the ratio of N_{exp}=N_{FE} of 1.04 and a coefficient of variation (COV) equal to 10.2%. The difference may be explained by the use of the nominal section properties and residual stresses pattern in the absence of measured experimental data.

Published in : J. Struct. Eng.(2024), 150(9), 04024122
DOI: 10.1061/JSENDH.STENG-12984
Status : Postprint (Author's version)

- The shell FE model gives higher results by 3.4% than the solid FE model for all imperfection shapes. It should also be noted that the influence of the element type to the member resistance is smaller when local buckling modes have been considered as initial imperfections.
- The residual stresses can reduce the member buckling capacity up to 7% for the cases where an initial flexural imperfection has been implemented. However, when a local or a torsional– flexural initial imperfection is adopted, it seems that their influence on the member's resistance is negligible (less than 0.5%).
- It can be seen that the influence of the magnitude of local buckling imperfection shapes (i.e., h=100 or h=50) to the member resistance is inconsequential (less than 0.5%).
- It has been observed that a flexural initial imperfection gives a lower resistance up to 7% compared with a torsional–flexural imperfection, even though the first buckling mode is the torsional–flexural one.
- For the cases where the local buckling mode is the relevant one, it has been shown that the flexural initial imperfection with value of L=700 gives a lower resistance up to 6.4% compared with a local imperfection with value of h=50 þ RS for the concentric loaded specimens and 1.6% for the eccentric ones. Subsequently, the influence of the imperfection shape is more significant for the centrally loaded members, while it is minimized when the load is eccentrically applied.
- The equivalent imperfection of L=700 with a flexural buckling eigenmode shape gives up to 3.5% higher results than those obtained for an imperfection of L=1,000 accompanied by residual stresses.

Table 2. Axial compression validation

Number	Buckling shape	Imperfection value	Element type	Axial compression force (kN)			
				L = 650 (mm)	L = 1,170 (mm)	L = 1,750 (mm)	L = 2,300 (mm)
1	Flexural	L=1,000	Shell	271.73	196.52	105.87	63.60
2	Flexural	L=1,000	Solid	274.56	197.77	104.42	62.90
3	Flexural	L=700	Shell	263.98	184.84	101.65	62.06
4	Flexural	L=700	Solid	266.77	185.56	100.24	61.12
5	Flexural	L=1,000 + RS	Shell	262.1	187.80	102.89	63.14
6	Flexural	L=5,000 + RS	Shell	280.8	217.57	113.83	66.76
7	Local	h=50	Shell	282.70	—	—	—
8	Local	h=50	Solid	280.29	—	—	—
9	Local	h=100	Shell	289.12	—	—	—
10	Local	h=100	Solid	285.87	—	—	—
11	Local	h=50 + RS	Shell	282.08	—	—	—
12	Experimental results (Spiliopoulos et al. 2018)			—	228.74	—	—

Table 3. Axial and strong axis bending validation

Number	Buckling shape	Imperfection value	Element type	Axial compression force (kN)			
				L = 650 (mm)	L = 1,170 (mm)	L = 1,750 (mm)	L = 2,300 (mm)
				$e_v = 22$	$e_v = 22$	$e_v = 30$	$e_v = 30$
1	Flexural	L=1,000	Shell	158.54	143.62	95.30	62.06
2	Flexural	L=1,000	Solid	154.62	139.39	92.25	60.42
3	Flexural	L=700	Shell	158.1	140.12	91.20	60.00
4	Flexural	L=700	Solid	154.06	136.04	88.46	58.42
5	Flexural	L=1,000 + RS	Shell	158.78	135.32	88.75	59.89
6	Flexural	L=5,000 + RS	Shell	177.13	166.06	109.6	66.79
7	Torsional–flexural	L=1,000	Shell	159.28	144.84	95.95	62.21
8	Torsional–flexural	L=1,000	Solid	155.45	140.39	92.80	60.57
9	Torsional–flexural	L=700	Shell	158.65	142.18	91.95	60.20
10	Torsional–flexural	L=700	Solid	155.24	137.46	89.11	58.61

Published in : J. Struct. Eng.(2024), 150(9), 04024122
DOI: 10.1061/JSENDH.STENG-12984
Status : Postprint (Author's version)

11	Torsional–flexural	L=1,000 + RS	Shell	159.51	144.93	95.60	61.82
12	Torsional–flexural	L=5000 + RS	Shell	177.25	165.83	110.3	66.875
13	Local	h=50	Shell	159.33	—	—	—
14	Local	h=50	Solid	156.21	—	—	—
15	Local	h=100	Shell	159.3	—	—	—
16	Local	h=100	Solid	156.09	—	—	—
17	Local	h=50 + RS	Shell	159.74	—	—	—
18	Experimental results (Spiliopoulos et al. 2018)			185.51	182.64	116.54	77.21
19				172.72	—	119.63	76.71
20				—	—	—	78.1

Table 4. Axial and weak axis bending (TIC) validation

Number	Buckling shape	Imperfection value	Element type	Axial compression force (kN)							
				L = 650 (mm)	L = 1,170 (mm)			L = 1,750 (mm)		L = 2,300 (mm)	
				e_u = 22	e_u = 5	e_u = 15	e_u = 22	e_u = 30	e_u = 5	e_u = 30	e_u = 5
1	Flexural	L=1,000	Shell	125.3	152.4	113.2	97.44	60.6	92.06	44.03	58.08
2	Flexural	L=1,000	Solid	123.1	149.2	111	95.46	59.13	89.73	43.04	57.63
3	Flexural	L=700	Shell	124.7	148	111.2	96.26	59.77	89.43	43.39	57.56
4	Flexural	L=700	Solid	122.5	144.7	109.1	94.28	58.44	87.26	42.42	56.27
5	Flexural	L= 1,000 + RS	Shell	124.4	146.5	110	94.85	59	88.89	42.88	57.37
6	Flexural	L=5,000 + RS	Shell	135.6	155.1	113.2	97.54	60.79	102.8	44.3	63.70
7	Local	h=50	Shell	126.2	—	—	—	—	—	—	—
8	Local	h=50	Solid	124.3	—	—	—	—	—	—	—
9	Local	h=100	Shell	126.4	—	—	—	—	—	—	—
10	Local	h=100	Solid	124.4	—	—	—	—	—	—	—
11	Local	h=50 + RS	Shell	126.8	—	—	—	—	—	—	—
12	Experimental results (Spiliopoulos et al. 2018)			139.8	165.2	125.9	101.3	55.13	125.6	38.79	76.47
13				134.6	—	123.4		56.69	114.0	40.99	84.60

Table 5. Axial and biaxial bending (TIC) validation

Number	Buckling shape	Imperfection value	Element type	Axial compression force (kN)			
				L = 650 (mm) e_z = 35	L = 1,170 (mm) e_z = 35	L = 1,750 (mm) e_z = 35	L = 2,300 (mm) e_z = 35
1	Flexural	L=1,000	Shell	95.13	81.75	61.38	45.09
2	Flexural	L=1,000	Solid	93.50	79.54	59.84	44.07
3	Flexural	L=700	Shell	95.01	81.10	60.55	44.47
4	Flexural	L=700	Solid	93.30	78.91	59.08	43.42
5	Flexural	L= 1,000 + RS	Shell	94.88	79.76	58.59	43.10
6	Flexural	L=5,000 + RS	Shell	94.35	81.83	61.75	45.27
7	Torsional–flexural	L=1,000	Shell	95.46	82.30	61.54	45.16
8	Torsional–flexural	L=1,000	Solid	93.85	79.93	59.97	44.12
9	Torsional–flexural	L=700	Shell	95.46	81.89	60.79	44.57
10	Torsional–flexural	L=700	Solid	93.68	79.49	59.27	43.50

Published in : J. Struct. Eng.(2024), 150(9), 04024122
DOI: 10.1061/JSENDH.STENG-12984
Status : Postprint (Author's version)

11	Torsional–flexural	L= 1,000 + RS	Shell	95.37	82.66	61.42	45.21
12	Torsional–flexural	L=5,000 + RS	Shell	95.46	82.72	61.72	45.35
13	Local	h=50	Shell	94.78	—	—	—
14	Local	h=50	Solid	94.25	—	—	—
15	Local	h=100	Shell	95.25	—	—	—
16	Local	h=50	Solid	94.13	—	—	—
17	Local	h=50 + RS	Shell	94.52	—	—	—
18	Experimental results (Spiliopoulos et al. 2018)			93.32	74.87	58.49	43.32
19				95.19	—	56.32	41.17

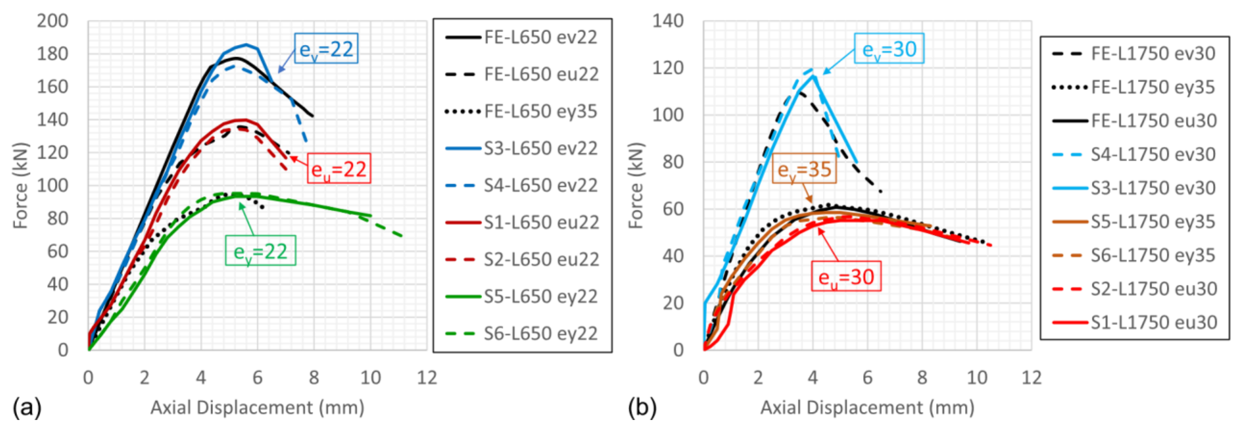

Fig. 9. Comparison between experimental and numerical results of Imp. L=5,000 þ RS for specimens with a buckling length of (a) 650 mm; and (b) 1,750 mm [experimental data from Spiliopoulos et al. (2018)].

Final Numerical Model

Based on the previous investigations, 4-node shell elements (type S4R) will be used hereafter to simulate the members, similarly to what was already done in previous research works (Dinis et al. 2019; Može et al. 2014). In addition, the boundary conditions will be simulated as previously described by attaching rigid constraints to the column end sections at pinned extremities. A bilinear material law as described in EN1993-1-5-Annex C and prEN 1993-1-14 clause 5.3.2 will also be adopted. Furthermore, only flexural buckling modes will be considered hereafter because it has been shown that torsional and flexural–torsional buckling modes can be disregarded for equal-leg angles, confirming thus the provisions of Annex F of prEN1993-3, while leg imperfections seem to be unimportant in the studied range. Therefore, for all load cases, the equivalent imperfection L=700 with a flexural buckling shape will be adopted; this imperfection gives consistent and safe results and therefore has been preferred for the following studies.

Results and Comparisons

Comparison of the Codes with the Numerical Analyses

In the following, a large number of numerical parametrical studies have been conducted by means of the full nonlinear software ABAQUS, using the final model described in the section "Final Numerical Model." Subsequently, the numerically

Published in : J. Struct. Eng.(2024), 150(9), 04024122
DOI: 10.1061/JSENDH.STENG-12984
Status : Postprint (Author's version)

obtained resistances have been compared with those resulting from the application of the codes. For all samples, the analytical load for the three provisions (prEN 1993-1-3, prEN 1993-3, ANSI/AISC 360-22) was determined using the nominal geometrical and material properties without safety factors.
Table 6 presents the details of the numerical samples such as the cross sections (covering all section classes), lengths, and steel grades. Although the first instability eigenmodes that result from an elastic buckling analysis are reported in this table, it should be said that initial imperfections implemented in the model were affine only to the first flexural buckling mode shape. For each sample, five loading cases have been considered as described in Table 6.
For each case, the load application point is shown in Fig. 10.

Member Subjected to Axial Compression

The numerical simulations have been performed by considering a concentric axial force applied at point P_1 in Fig. 10(a). Fig. 11 illustrates the interaction ratio of ($N_{code}/N_{c,Rk} + \Delta M_{v,code}=M_{v,Rk}$) for both prEN 1993-1-3 and prEN 1993-3, and the ratio ($N_{code}= Q \cdot A \cdot F_y$) for the ANSI/AISC 360-22 versus the weak axis slenderness $\bar{\lambda}_v$. As already explained, ANSI/AISC 360-22 does not account for the additional bending moment ΔM resulting of the shift of the centroid. The ratio ($N_{FE}=Af_y$) for the numerical results versus the weak axis slenderness is also reported. As expected, both prEN 1993-3 and prEN 1993-1-3 give almost the same results, while AISC seems to provide higher resistances than the European provisions. Finally, the numerical results are higher for lower slenderness and in between the American and European provisions for the higher ones.
Fig. 12 presents the ratio ($N_{code}=N_{FE}$) for the three provisions, as well as their corresponding mean values m versus the weak axis slenderness $\bar{\lambda}_v$. It can be seen that both prEN 1993-3 and prEN 1993-1-3 give identical results for class-3 profiles, while they have minor differences for the class-4 ones. There is only one case where prEN 1993-3 and prEN1993-1-3 predict a higher resistance than the numerical one, with a deviation of 0.5%. However, this is acceptable, considering that strain hardening was neglected in the numerical analyses. Despite the small differences, it can be observed that the three provisions give almost the same mean values of m–s for axially compressed members, with the American ones predicting more results in the unsafe zone with a max standard deviation of 6.3%.

Member Subjected to Axial Force and Strong Axis Bending

For this case, the axial force is applied with an eccentricity along the minor principal axis v–v [point P_2 in Fig. 10(b)] that ranges between 5.0 and 35.0 mm, depending on the profile geometry. Fig. 13 illustrates the interaction ratio ($N_{code}/N_{c,Rk} + M_{u,code}/M_{v,Rk} + \Delta M_{v,code}=M_{v,Rk}$) for both prEN 1993-1-3 and prEN 19933, as well as the ratio ($N_{code}=Q \cdot A \cdot F_y$ þ $M_{u;code}=M_{plw}$) for the ANSI/AISC 360-22 provisions versus the weak axis slenderness $\bar{\lambda}_v$. The ratio ($N_{FE}=Af_y$ þ $M_{u;FE}=W_{pl;u}f_y$) for the numerical results is also reported.

Fig. 14 presents the ratio ($N_{code}=N_{FE}$) for the three studied provisions and their mean values of members subjected to axial compression force and strong axis bending, versus the nondimensional slenderness $\bar{\lambda}_v$. For all samples, the weak axis check was the critical one. It can be seen that all results are on the safe side, with the ones given by prEN 1993-1-3 to be the most conservative and having the bigger scatter. It may also be observed that both prEN 1993-3 and ANSI/AISC 360-22 give similar mean values.

Member Subjected to Axial Force and Weak Axis Bending

The numerical investigations have been performed by implementing an eccentric axial force on the u–u axis [point P_3in Fig. 10(c)], that ranges randomly between 5.0 and 35.0 mm. Fig. 15 illustrates the interaction ratio of ($N_{code}=N_{c;Rk}$ þ $M_{v;code}=M_{v;Rk}$ þ $\Delta M_{v;code}= M_{v;Rk}$) for both prEN 1993-1-3 and prEN 1993-3, as well as the ratio ($N_{code}=Q \cdot A \cdot F_y$ þ $M_{v;code}=M_{plz}$) for AISC 360-22. The interaction ratio ($N_{FE}=A \cdot F_y$ þ $M_{v;FE}=W_{pl;v}f_y$) for the numerical results versus weak axis slenderness $\bar{\lambda}_v$ is also presented.

Published in : J. Struct. Eng.(2024), 150(9), 04024122
DOI: 10.1061/JSENDH.STENG-12984
Status : Postprint (Author's version)

The ratio (N_{code}=N_{FE}) for the three provisions, as well as their mean values for the case where the member is subjected to axial compression force and weak axis bending (TIC), versus nondimensional slenderness $\bar{\lambda}_v$, is shown in Fig. 16. Again, the weak axis check was the critical one for all the samples. The imperfection shape has been taken in order to produce compression force in the tips at the initial state. As previously stated, prEN 1993-1-3 seems to give the most conservative results, with AISC 360-22 predicting a slightly higher resistance of the member compared to prEN 1993-3.

Member Subjected to Axial Force and Weak Axis Bending

For this case, the numerical samples were subjected to an eccentric axial force on the u–u axis [point P_4 in Fig. 10(d)] that ranges between –5.0 and –35.0 mm. The imperfection shape has been taken such as it produces a tension force in the tips at the initial state. Fig. 17 illustrates the interaction ratio of ($N_{code}/N_{c;Rk}$ +$M_{v;code}/M_{v;Rk}$+$\Delta M_{v;code}/M_{v;Rk}$) for both prEN 1993-1-3 and prEN 1993-3 versus weak axis slenderness $\bar{\lambda}_v$. The ratio ($N_{code}/Q \cdot A \cdot F_y$ + $M_{v;code}/M_{plz}$) for the AISC 360-22 as well as the ratio ($N_{FE}/A \cdot F_y$ + $M_{v;FE}/M_{v;pl}$) for the numerical results are also included.
Fig. 18 shows the ratio (N_{code}/N_{FE}) for the three provisions, when the member is subjected to axial compression force and weak axis bending [tip in tension (TIT)] versus nondimensional slenderness $\bar{\lambda}_v$; their mean values are also presented. For the case when the tip is in compression, prEN 1993-1-3 gives the most conservative results compared to the other two provisions. AISC 360-22 predicts a slightly higher resistance of the member compared to prEN 1993-3, but always on the safe side (the one result in the unsafe area can be accepted for the reasons explained in previous subsections).

Member Subjected to Axial Force and Biaxial Bending

For the samples that are subjected to biaxial bending, the axial force is applied on its midheight of the leg on an eccentric point about the z–z axis [point P_5 in Fig. 10(e)]. This point could represent the position of the connecting bolt for angles in structures. Fig. 19 illustrates the relation between the interaction ratio of ($N_{code}/N_{c,Rk}$ + $M_{u,code}/M_{u,Rk}$ + ($M_{v,code}$ + $\Delta M_{v,code}$)/$M_{v,pRk}$) for prEN 1993-1-3 and prEN 1993-3, ($N_{code}/Q \cdot A \cdot F_y$ + $M_{u,code}/M_{plw}$ + $M_{v,code}/M_{plz}$) for the AISC 360-22 provisions, as well as the ratio (N_{FE}/Af_y + $M_{u,FE}/W_{pl,u}f_y$ + $M_{v,FE}/W_{pl,v}f_y$) for the numerical results, versus the slenderness $\bar{\lambda}_v$.
Fig. 20 presents a comparison of the numerical and analytical resistances (N_{code}=N_{FE}) for the provisions of the three normative documents for these members, versus nondimensional slenderness $\bar{\lambda}_v$. The weak axis check was also the critical one for this loading case, and all the members buckled toward their weak axis. The prEN 1993-1-3 provisions again seem to be the most conservative in terms of mean value but have a bigger deviation. On the contrary, the scatter is much less for the other two provisions, with the mean value of both AISC 360-22 specification and prEN 1993-3 to be quite close.

Summary

From the presented study, it may be concluded that this specific provision of prEN 1993-1-3 reported in clause 8.2.5 about the interaction formulae given for the buckling resistance of a member subjected to compression and biaxial bending may be applied for hot-rolled members, but looks to be quite conservative compared to other available normative documents, such as the prEN 1993-3 or AISC 360-22 provisions.
Table 7 summarizes the mean m and standard deviation s values of the ratio (N_{code}=N_{FE}) for the three considered documents and for all the studied cases. It can be observed that the mean values of AISC 360-22 and prEN 1993-3 are quite close, with prEN 19933 having slightly smaller deviations.

Comparison of the Codes with the Experimental Tests

In this part, the previously given design formulas are checked against the experimental tests of Spiliopoulos et al. (2018). The analytical load for the three aforementioned provisions was determined using the experimental material properties from the same literature.

Table 8 summarizes the ratio (N_{code}=N_{exp}) for the experimental tests in regard to the three provisions. It seems again that prEN 1993-1-3 gives the most conservative results, while all three codes provide safe results.

Table 6. Load cases for concentric and eccentric axial loaded members

					Load cases				
					N_{Ed}	$M_{u,Ed}$		$M_{v,Ed}$	$M_{u,Ed}$
							e_u (TIC) (mm)		
Number	Angle profile	Length (mm)	1st buckling mode	f_y (N/mm^2)	e (mm)	e_v (mm)	e_u	(TIT) (mm)	e_z (TIC) (mm)
1	45 × 45 × 3	1,000	Flexural	355	0	10	10	-10	14.14
2	45 × 45 × 3	1,000	Flexural	460	0	10	10	-10	14.14
3	45 × 45 × 3	2,000	Flexural	355	0	10	10	-10	14.14
4	45 × 45 × 3	2,000	Flexural	460	0	10	10	-10	14.14
5	70 × 70 × 5	1,000	Local	355	0	5	5	-5	7.07
6	70 × 70 × 5	1,000	Local	460	0	5	5	-5	7.07
7	70 × 70 × 5	2,000	Flexural	355	0	20	20	-20	28.28
8	70 × 70 × 5	2,000	Flexural	460	0	20	20	-20	28.28
9	70 × 70 × 6	1,000	Flexural	355	0	35	35	-35	49.50
10	70 × 70 × 6	1,000	Flexural	460	0	35	35	-35	49.50
11	70 × 70 × 6	2,000	Flexural	355	0	35	35	-35	49.50
12	70 × 70 × 6	2,000	Flexural	460	0	35	35	-35	49.50
13	70 × 70 × 7	650	Local	235	0	22	22	-22	35
14	70 × 70 × 7	1,170	Flexural	235	0	22	5	-5	35
15	70 × 70 × 7	1,170	Flexural	235	0	22	15	-15	35
16	70 × 70 × 7	1,170	Flexural	235	0	22	22	-22	35
17	70 × 70 × 7	1,750	Flexural	235	0	30	30	-30	35
18	70 × 70 × 7	1,750	Flexural	235	0	30	5	-5	35
19	70 × 70 × 7	2,300	Flexural	235	0	30	30	-30	35
20	70 × 70 × 7	2,300	Flexural	235	0	30	5	-5	35
21	80 × 80 × 5	2,000	Flexural	355	0	25	25	-25	35.36
22	80 × 80 × 5	2,000	Flexural	460	0	25	25	-25	35.36
23	80 × 80 × 5	3,000	Flexural	355	0	25	25	-25	35.36
24	80 × 80 × 5	3,000	Flexural	460	0	25	25	-25	35.36
25	150 × 150 × 14	2,000	Flexural	355	0	12	12	-12	16.97
26	150 × 150 × 14	2,000	Flexural	460	0	12	12	-12	16.97
27	150 × 150 × 14	3,000	Flexural	355	0	20	20	-20	28.28
28	150 × 150 × 14	3,000	Flexural	460	0	20	20	-20	28.28
29	150 × 150 × 18	2,000	Flexural	355	0	10	10	-10	14.14
30	150 × 150 × 18	2,000	Flexural	460	0	10	10	-10	14.14
31	150 × 150 × 18	3,000	Flexural	355	0	32	32	-32	45.25
32	150 × 150 × 18	3,000	Flexural	460	0	32	32	-32	45.25
33	250 × 250 × 20	2,000	Local	355	0	8	8	-8	11.31
34	250 × 250 × 20	2,000	Local	460	0	8	8	-8	11.31
35	250 × 250 × 2	3,000	Local	355	0	12	12	-12	16.97
36	250 × 250 × 20	3,000	Local	460	0	12	12	-12	16.97
37	250 × 250 × 22	2,000	Local	355	0	5	5	-5	7.07
38	250 × 250 × 22	2,000	Local	460	0	5	5	-5	7.07
39	250 × 250 × 22	3,000	Flexural	355	0	5	5	-5	7.07
40	250 × 250 × 22	3,000	Flexural	460	0	5	5	-5	7.07

Published in : J. Struct. Eng.(2024), 150(9), 04024122
DOI: 10.1061/JSENDH.STENG-12984
Status : Postprint (Author's version)

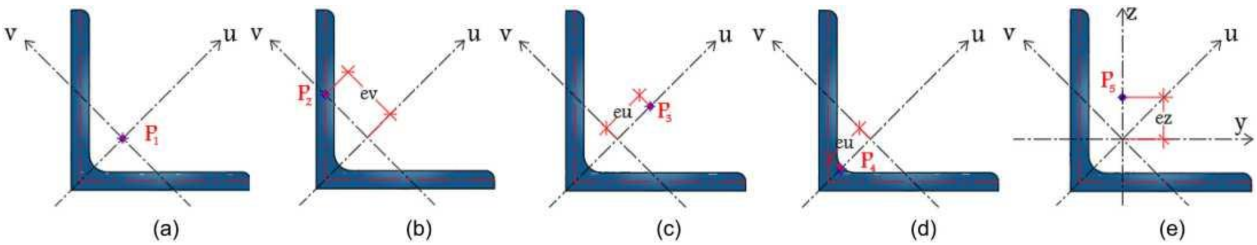

Fig. 10. Position of the load application point for the samples subjected to: (a) *N*; (b) *N* + *Mu*; (c) *N* + M_v (TIC); (d) *N* + M_v (TIT); and (e) *N* + *Mu* + *Mv* (TIC).

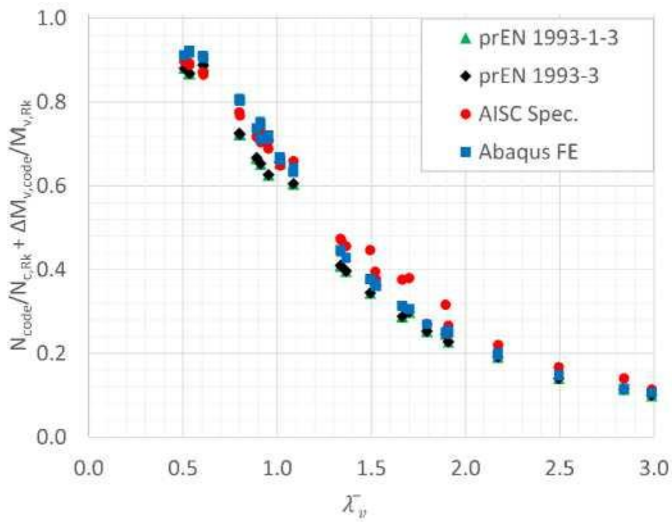

Fig. 11. Interaction ratio for members subjected to axial compression force (codes results).

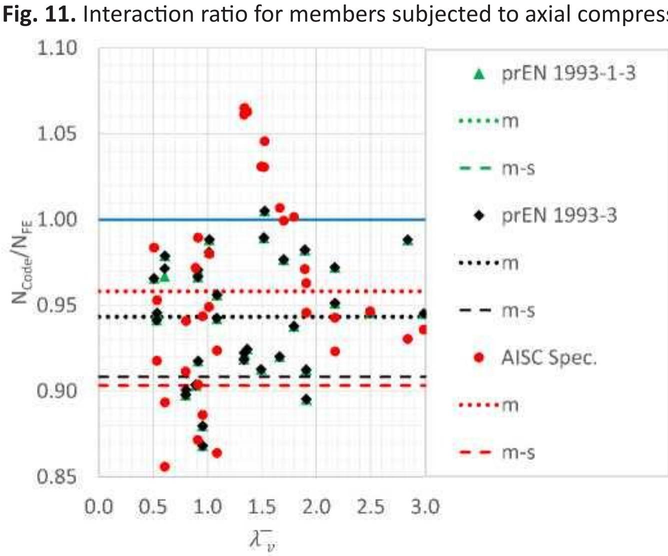

Fig. 12. Comparison between N $_{code}$ =N $_{FE}$ ratio for members subjected to axial compression force.

Published in : J. Struct. Eng.(2024), 150(9), 04024122
DOI: 10.1061/JSENDH.STENG-12984
Status : Postprint (Author's version)

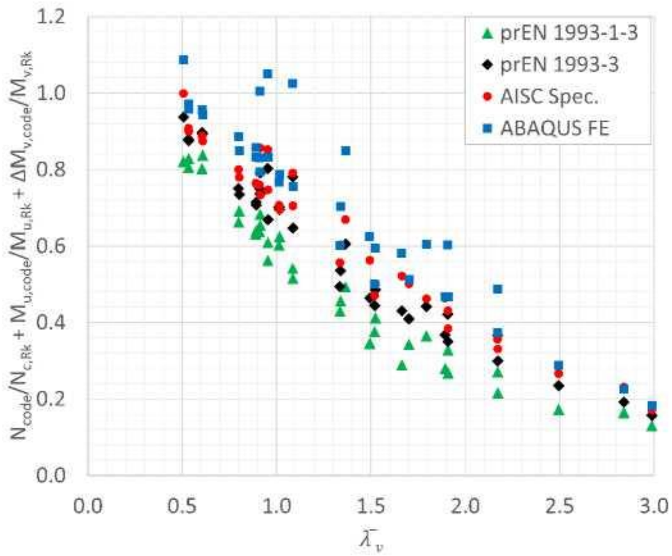

Fig. 13. Interaction ratio for members subjected to N + Mu.

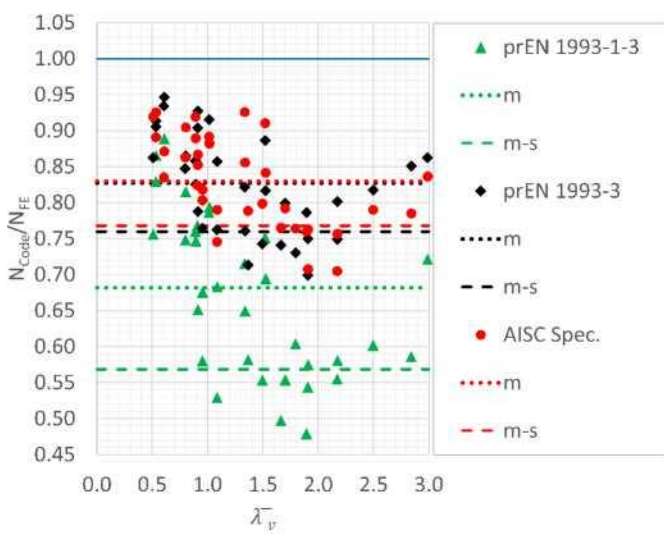

Fig. 14. Comparison between $N_{code} = N_{FE}$ ratio for members subjected to N + M_u.

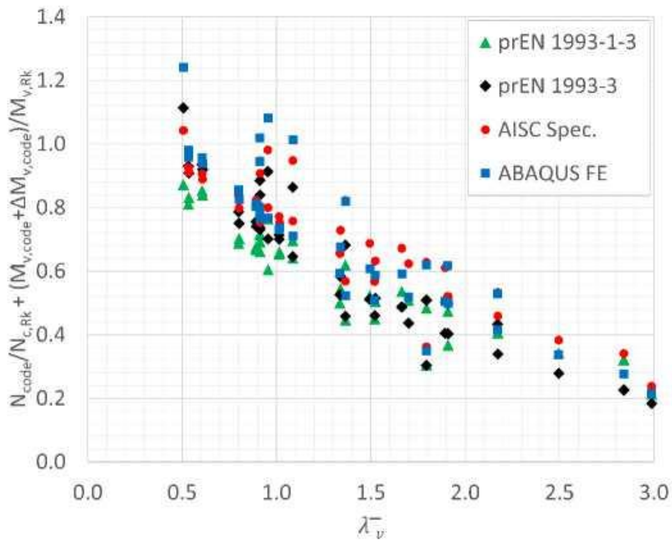

Fig. 15. Interaction ratio for members subjected to N + M_v (TIC).

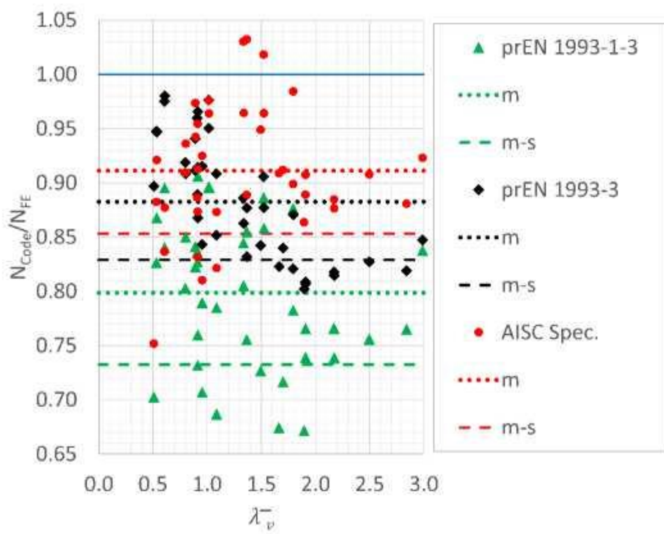

Fig. 16. Comparison between N $_{code}$ =N $_{FE}$ ratio for members subjected to N + M_v (TIC).

Published in : J. Struct. Eng.(2024), 150(9), 04024122
DOI: 10.1061/JSENDH.STENG-12984
Status : Postprint (Author's version)

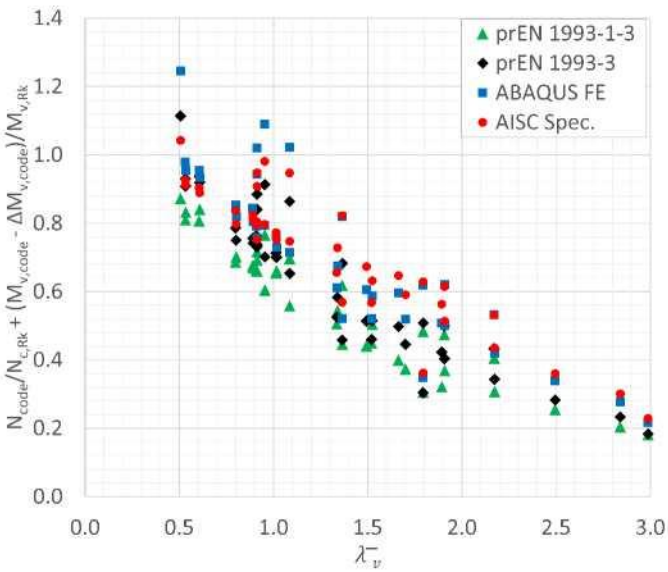

Fig. 17. Interaction ratio for members subjected to N + M_v (TIT).

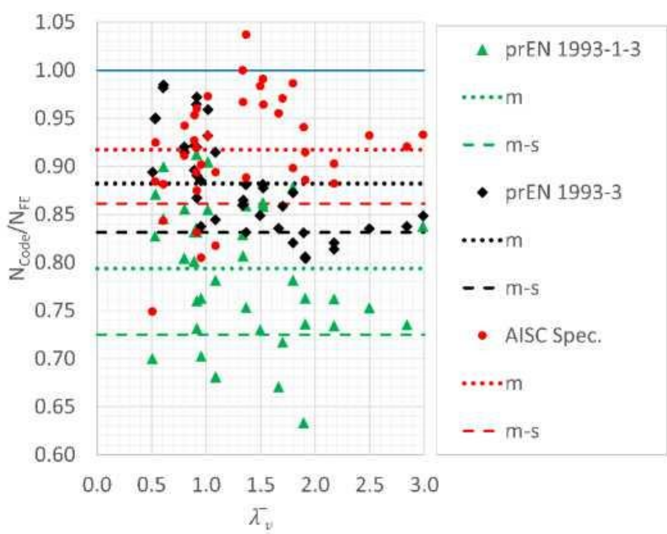

Fig. 18. Comparison between N_{code} |NFE ratio for members subjected to N + M_v (TIT).

Published in : J. Struct. Eng.(2024), 150(9), 04024122
DOI: 10.1061/JSENDH.STENG-12984
Status : Postprint (Author's version)

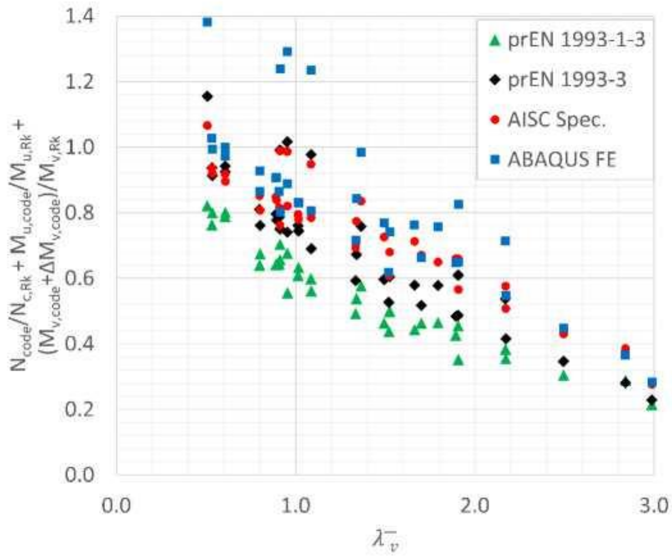

Fig. 19. Interaction ratio for members subjected to N + My (TIC).

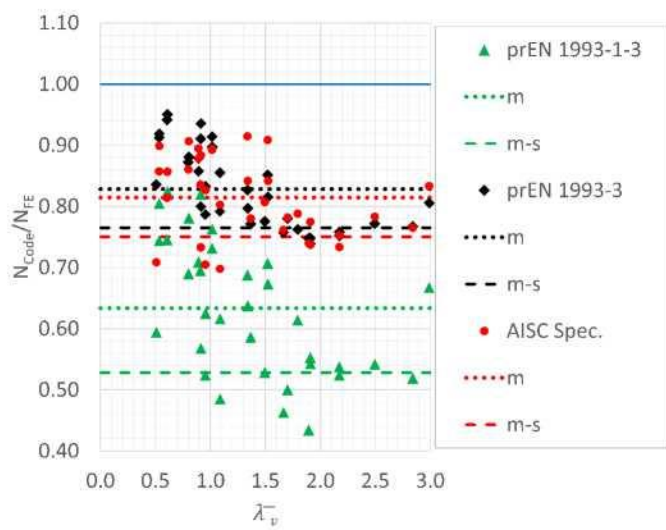

Fig. 20. Comparison between N_{code} |NFE ratio for members subjected to N + My (TIC).

Table 7. Mean and standard deviation ofN =N ratio for all load cases

Loading case	Statistical parameters	prEN 1993-1-3	prEN 1993-3	AISC 360-22
Axial	m	0.94	0.94	0.96
	s (%)	3.5	3.5	5.5
Axial+ strong bending	m	0.68	0.83	0.83
	s (%)	11.4	6.8	6.2
Axial + weak bending (TIC)	m	0.80	0.88	0.91
	s (%)	6.6	5.4	5.8
Axial + weak bending (TIT)	m	0.79	0.88	0.92
	s (%)	6.9	5.1	5.6

Published in : J. Struct. Eng.(2024), 150(9), 04024122
DOI: 10.1061/JSENDH.STENG-12984
Status : Postprint (Author's version)

Axial + Bi bending (TIC)	m	0.63	0.83	0.81
	s (%)	10.6	6.3	6.4

Table 8. Ratio of N_{code}=N_{exp} for all validated cases

Sample		prEN 1993-1-3	prEN 1993-3	AISC 360-22
L (mm)	Eccentricity (mm)			
650	e_v = 22	0.626	0.747	0.799
650	eu = 22	0.625	0.805	0.690
650	e_y = 35	0.566	0.832	0.715
1,170	e = 0	0.725	0.725	0.806
1,170	ev = 22	0.470	0.573	0.624
1,170	eu = 5	0.740	0.794	0.873
1,170	eu = 15	0.687	0.777	0.806
1,170	eu = 22	0.707	0.812	0.819
1,170	ey = 35	0.613	0.850	0.802
1,750	e_v = 30	0.438	0.539	0.577
1,750	eu = 30	0.816	0.877	0.955
1,750	eu = 5	0.639	0.643	0.747
1,750	e_y = 35	0.623	0.801	0.819
2,300	ev = 30	0.478	0.577	0.583
2,300	eu = 30	0.864	0.886	0.973
2,300	eu = 5	0.630	0.620	0.682
2,300	ey = 35	0.660	0.800	0.826
m		0.642	0.744	0.770
s (%)		11.07	10.86	11.10

Conclusions

This study investigates the resistance and stability of single-angle members from hot-rolled class 1–4 sections that are subjected to concentric and eccentric loading. Numerical parametrical studies have been conducted with the full nonlinear software ABAQUS, considering geometrical and material nonlinearities, and the influence of different modeling parameters has been investigated. The numerical model has been validated through comparisons with experimental tests available from the literature. Subsequently, the numerical results have been compared with the relevant predictions of three different normative documents: (1) prEN 1993-1-3, (2) prEN 1993-3, and (3) ANSI/AISC 360-22 specification. From these numerical and analytical investigations, the following conclusions may be drawn:

- The shell FE models gave higher results up to 3.4% than the solid FE models for all considered imperfection shapes. As the difference remains low, the simplified modeling of an angle section with shell elements could be acceptable for the prediction of the failure load and mode.
- The residual stresses can reduce the member buckling capacity up to 7% for the cases where an initial flexural imperfection has been implemented.
- It has been observed that the influence of the magnitude of local buckling imperfection shapes (i.e., h=100 or h=50) to the member resistance is negligible (less than 0.5%).
- It has been observed that a flexural initial imperfection gives a lower resistance up to 7% compared with a torsional–flexural imperfection, even though the first buckling mode is the torsional–flexural one.
- The equivalent imperfection value of L=700 with a flexural buckling eigenmode shape looks to be a good assumption to be easily used to calculate the member failure load because it gives up to 3.5% higher results than the value of L=1000 þ RS in the ABAQUS analysis.
- It has been shown that the buckling member resistance should be based on the flexural modes only, even though the relevant elastic buckling mode is a local or a torsional–flexural one.

Published in : J. Struct. Eng.(2024), 150(9), 04024122
DOI: 10.1061/JSENDH.STENG-12984
Status : Postprint (Author's version)

- It has been shown that the specific provision of prEN 1993-1-3 reported in clause 8.2.5 about the interaction formulae given for the buckling resistance of a member subjected to compression and biaxial bending may be safely applied for hot-rolled members but looks to be quite conservative compared to other available normative documents.
- The provisions of prEN 1993-3 give almost the same mean value of the American standard AISC 360-22 specification for the considered numerical samples.

Data Availability Statement

Some or all data that support the findings of this study are available from the corresponding author upon reasonable request.

Notation

The following symbols are used in this paper:

A, A_{eff} = gross and effective area of the cross section; C_b = lateral–torsional buckling modification factor (AC);
c = outstand flange width (c ¼ h-t-r_2);

E = modulus of elasticity; e, e_u, e_v, e_z = load eccentricity;

F_y = specified minimum yield stress of steel (AC);
F_n, F_e = nominal strength and Euler stress for compression member (AC);
f_y, f_{yb}, f_{ya} = basic and average yield strength of the
material;
K = buckling factor for compression member (AC);

h = angle leg width;

k_σ = plate buckling factor;
L = length (member length, span length etc.);

$M_{cu;Rd}$, $M_{cv;Rd}$ = design value of the cross-sectional resistance to the bending moment about the u–u and v–v axis, respectively;

$M_{nw;LB}$, $M_{nw;LTB}$ = nominal flexural strength for local and lateral–torsional buckling (AC);
M_{nw}, M_{nz} = nominal flexural strength about the strong and weak axis, respectively (AC);

M_{plw}, M_{plz} = plastic flexural strength about the strong and weak axis, respectively (AC);

$M_{u;code}$, $M_{v;code}$ = required flexural strength about the strong and weak axis, respectively, per code;

$\Delta M_{u;code}$, $\Delta M_{v;code}$ = additional bending moment about the strong and weak axis, respectively, due to the centroidal shift of class-4 sections;

$M_{u,Ed}$, $M_{v,Ed}$ = design bending moment about the u–u and
v–v axis, respectively;

$\Delta M_{u,Ed}$, $\Delta M_{v,Ed}$ = additional bending moment about the u–u and v–v axis respectively, due to the centroidal shift of the effective cross section;

$M_{u,Rd}$ = characteristic value of the cross-sectional resistance to the bending moment;

$M_{u,Rk}$, $M_{v,Rk}$ = characteristic value of the cross-sectional resistance of a member in the bending
moment about the u–u and v–v axis respectively;
M_{uw}, M_{uz} = required flexural strength about the strong and weak axis, respectively (AC); M_y = yield moment (AC);

$N_{c,Rd}$, $N_{c,Rk}$ = design and characteristic values of the cross-sectional resistance of a member in compression;

N_{code}, N_{FE} = design axial force per code and numerical design resistance;
P_u, P_n, = required and nominal axial strength (AC);

Published in : J. Struct. Eng.(2024), 150(9), 04024122
DOI: 10.1061/JSENDH.STENG-12984
Status : Postprint (Author's version)

Q = reduction factor for plate buckling (AC); r = radius of gyration (AC);
r_1, r_2 = radius of root and toe fillet;
S_c = elastic section modulus for bending (AC);
$W_{eff;u}$, $W_{eff;v}$ = effective section modulus for bending about the u–u and v–v axis, respectively;
$W_{el;u}$, $W_{el;v}$ = elastic section modulus for bending about the u–u and v–v axis, respectively;
$W_{pl;u}$, $W_{pl;v}$ = plastic section modulus for bending about the u–u and v–v axis, respectively;
γ_{M0} = material safety factor that equals 1.0 as recommended by EN 1993-1-1;
ε = material parameter depending on f_y, equals $\varepsilon = \sqrt{235/f_y[N/\text{mm}^2]}$
$\bar{\lambda}$ = relative slenderness for flexural buckling;
$\bar{\lambda}_p$, $\bar{\lambda}_{p,red}$ = relative and reduced relative plate slenderness for plate buckling;
$\bar{\lambda}_{LT}$, $\bar{\lambda}_{LT,red}$ = relative and reduced relative slenderness for lateral–torsional buckling;
λ_c= slenderness parameter for flexural buckling (AC);
ρ, ρ_e = reduction factor for plate buckling and
Euler's elastic reduction factor; σ_{cr}, $\sigma_{com;Ed}$ = critical and design compressive stress for plate buckling, respectively;
χ_u, χ_v, χ_{TF}, χ_{LT} = buckling reduction factors;
Φ, Φ_b = resistance factors for compression and flexure (AC); and
ψ = ratio of end moments in a beam, ratio of end stresses of the compression plate.

References

ANSI/AISC (American Institute of Steel Construction). 2022. Specification for structural steel buildings. ANSI/AISC 360-22. Chicago: ANSI.

Ban, H. Y., G. Shi, Y. J. Shi, and Y. Q. Wang. 2013. "Column buckling tests of 420MPa high strength steel single equal angles." Int. J. Struct. Stab. Dyn. 13 (2): 1250069. https://doi.org/10.1142/S02194554125 00691.

Behzadi-Sofiani, B., L. Gardner, and M. A. Wadee. 2021. "Stability and design of fixed-ended stainless steel equal-leg angle section compression members." Eng. Struct. 249 (Dec): 113281. https://doi.org/10.1016 /j.engstruct.2021.113281.

Bezas, M.-Z. 2022. "Design of lattice towers from hot-rolled equal leg steel angles." Ph.D. thesis, Dept. of Urban and Environmental Engineering, Univ. of Liège and National Technical Univ. of Athens.

Bezas, M.-Z., J. F. Demonceau, I. Vayas, and J.-P. Jaspart. 2021a. "Classification and cross-section resistance of equal-leg rolled angle profiles." J. Constr. Steel Res. 185 (Aug): 106842. https://doi.org/10.1016/j.jcsr .2021.106842.

Bezas, M.-Z., J. F. Demonceau, I. Vayas, and J.-P. Jaspart. 2021b. "Experimental and numerical investigations on large angle high strength steel columns." Thin-Walled Struct. 159 (Feb): 107287. https://doi.org /https://doi.org/10.1016/j.tws.2020.107287.

Bezas, M.-Z., J. F. Demonceau, I. Vayas, and J.-P. Jaspart. 2022. "Design rules for equal-leg angle members subjected to compression and bending." J. Constr. Steel Res. 189 (Feb): 107092. https://doi.org/https://doi .org/10.1016/j.jcsr.2021.107092.

BS (British Standard). 2008. Execution of steel structures and aluminium structures—Part 2. BS EN 1090-2. London: BS.

CEN (Comité Européen de Normalisation). 1994. Structural steel equal and unequal leg angles—Part 2. Tolerances on shapes and dimensions. EN 10056-2. Brussels, Belgium: CEN.

CEN (Comité Européen de Normalisation). 2005. Design of steel structures—Part 1-1.2005. General rules and rules for buildings. EN 1993-1-1. Brussels, Belgium: CEN.

CEN (Comité Européen de Normalisation). 2006a. Design of steel structures—Part 1-5. Plated structures elements. EN 1993-1-5. Brussels, Belgium: CEN.

CEN (Comité Européen de Normalisation). 2006b. Design of steel structures—Part 3.2006. Towers, Masts and Chimneys. Tower and masts. EN 1993-3-1. Brussels, Belgium: CEN.

CEN (Comité Européen de Normalisation). 2006c. Eurocode 3: Design of steel structures—Part 1-3.2006. General rules—Supplementary rules for cold-formed members and sheeting. EN 1993-1-3. Brussels, Belgium: CEN.

CEN (Comité Européen de Normalisation). 2012. Overhead electrical lines exceeding Ac 1 kV—Part 1: General requirements—Common specifications. EN 50341-1 2012. Brussels, Belgium: CEN.

CEN (Comité Européen de Normalisation). 2020. Eurocode 3: Design of steel structures—Part 1-3. General rules—Supplementary rules for cold-formed members and sheeting. prEN 1993-1-3. Brussels, Belgium: CEN.

Published in : J. Struct. Eng.(2024), 150(9), 04024122
DOI: 10.1061/JSENDH.STENG-12984
Status : Postprint (Author's version)

CEN (Comité Européen de Normalisation). 2021. Design of steel structures—Part 3.2021. Towers, masts and chimneys. prEN 1993-3. Brussels, Belgium: CEN.

CEN (Comité Européen de Normalisation). 2022. Design of steel structures—Part 1-14.2018. Design assisted by finite element analysis. FprEN1993-1-1. Brussels, Belgium: CEN.

De Menezes, A. A., D. S. Vellasco, P. C. G. De Lima, and A. T. Da Silva. 2019. "Experimental and numerical investigation of austenitic stainless steel hot-rolled angles under compression." J. Constr. Steel Res. 152 (Apr): 42–56. https://doi.org/https://doi.org/10.1016/j.jcsr.2018.05 .033.

Dinis, P. B., D. Camotim, and A. Landesmann. 2019. "Design of simply supported hot-rolled steel short-to-intermediate angle columns." Steel Constr. 12 (4): 278–290. https://doi.org/https://doi.org/10.1002/stco .201900029.

ECCS (European Convention for Constructional Steelwork). 1976. Manual on stability of steel structures. Brussels, Belgium: ECCS.

Farhoud, H. 2022. "Design of members from class 1 to 4 equal leg angles according to the provisions of EN1993-1-3 and EN1993-3, Annex F." Master's thesis, Analysis and Design of Earthquake Resistant Structures, National Technical Univ. of Athens.

Fisher, J. M. 2000. Load and resistance factor design specification for singleangle members. Chicago: American Institute of Steel Construction.

Kettler, M., and H. Unterweger. 2019. "Laboratory tests on bolted steel angles in compression with varying end support conditions." [In German.] Stahlbau 88 (5): 447–459. https://doi.org/https://doi.org/10.1002/stab .201900013.

Liang, Y., V. V. K. Jeyapragasam, L. Zhang, and O. Zhao. 2019. "Flexuraltorsional buckling behaviour offixed-ended hot-rolled austenitic stainless steel equal-leg angle section columns." J. Constr. Steel Res. 154 (Mar): 43–54. https://doi.org/https://doi.org/10.1016/j.jcsr.2018.11.019.

Može, P., L.-G. Cajot, F. Sinur, K. Rejec, and D. Beg. 2014. "Residual stress distribution of large steel equal leg angles." Eng. Struct. 71 (Jul): 35–47. https://doi.org/10.1016/j.engstruct.2014.03.040.

Shi, G., Z. Liu, H. Ban, Y. Zhang, Y. Shi, and Y. Wang. 2012. "Tests and finite element analysis on the local buckling of 420 MPa steel equal angle columns under axial compression." Steel Compos. Struct. 12 (1): 31–51. https://doi.org/10.12989/scs.2012.12.1.031.

Shifferaw, Y., and B. W. Schafer. 2014. "Cold-formed steel lipped and plain angle columns with fixed ends." Thin-Walled Struct. 80 (Jul): 142–152. https://doi.org/10.1016/j.tws.2014.03.001.

Spiliopoulos, A., M. E. Dasiou, P. Thanopoulos, and I. Vayas. 2018. "Experimental tests on members made from rolled angle sections." Steel Constr. Des. Res. 11 (1): 84–93. https://doi.org/10.1002/stco .201710023.

Vayas, I., A. Charalampakis, and V. Koumousis. 2009. "Inelastic resistance of angle sections subjected to biaxial bending and normal forces." Steel Constr. Des. Res. 2 (2): 138–146. https://doi.org/10.1002/stco .200910018.

Vayas, I., J. P. Jaspart, A. Bureau, M. Tibolt, S. Reygner, and M. Papavasiliou. 2021. "Telecommunication and transmission lattice towers from angle sections—The ANGELHY project." ce/papers 4 (2–4): 210–217. https://doi.org/10.1002/cepa.1283.